

## Shear-induced phase transition and critical exponents in three-dimensional fiber networks

Sadjad Arzash<sup>1,2</sup>, Jordan L. Shivers,<sup>1,2</sup> and Fred C. MacKintosh<sup>1,2,3</sup><sup>1</sup>Department of Chemical & Biomolecular Engineering, Rice University, Houston, Texas 77005, USA<sup>2</sup>Center for Theoretical Biological Physics, Rice University, Houston, Texas 77030, USA<sup>3</sup>Departments of Chemistry and Physics & Astronomy, Rice University, Houston, Texas 77005, USA

(Received 7 May 2021; revised 7 July 2021; accepted 29 July 2021; published 17 August 2021)

When subject to applied strain, fiber networks exhibit nonlinear elastic stiffening. Recent theory and experiments have shown that this phenomenon is controlled by an underlying mechanical phase transition that is critical in nature. Growing simulation evidence points to non-mean-field behavior for this transition and a hyperscaling relation has been proposed to relate the corresponding critical exponents. Here, we report simulations on two distinct network structures in three dimensions. By performing a finite-size scaling analysis, we test hyperscaling and identify various critical exponents. From the apparent validity of hyperscaling, as well as the non-mean-field exponents we observe, our results suggest that the upper critical dimension for the strain-controlled phase transition is above three, in contrast to the jamming transition that represents another athermal, mechanical phase transition.

DOI: [10.1103/PhysRevE.104.L022402](https://doi.org/10.1103/PhysRevE.104.L022402)

Networks of interconnected fibers are common in both natural and synthetic contexts, with examples ranging from biopolymer networks to paper and carbon nanotube materials [1–3]. In biology, fibrous networks are primarily responsible for the mechanical stability of cells and tissues. These networks include both intracellular structures of actin and microtubules as well as extracellular matrices such as collagen and fibrin [4,5]. In recent decades, high-precision rheology experiments on purified, reconstituted biopolymer networks have revealed unusual elastic properties including negative normal stresses [6] and nonlinear strain stiffening [7,8]. It has been shown that the mechanics of such networks depend not only on the elasticity of individual fibers but also strongly on network connectivity. To understand the mechanical behavior of stiff biopolymer networks, coarse-grained athermal fiber models with controlled connectivity  $z$  have been used in the literature [9–15]. Strikingly, these simple models can accurately explain the strain stiffening observed in collagen experiments [16,17]. Both experiments and theory point to the importance of a mechanical phase transition as a function of strain.

Here, we study the critical aspects of this phase transition in three-dimensional (3D) fiber networks under an applied simple shear. Most prior systematic studies have been limited to 2D, due to the significant computational challenges imposed by the nonlinear elasticity and the need for large systems because of the diverging correlation length. Although models to date point to qualitatively similar behavior in 2D and 3D [16,18–20], important questions remain, e.g., concerning the possibility of non-mean-field behavior that has been observed in 2D. We show that fiber networks exhibit non-mean-field behavior in 3D and are consistent with a recently identified hyperscaling scaling relation [21], suggesting that the upper critical dimension for fiber networks is greater than three, in contrast to the jamming transition [22].

*Model.* We consider two varieties of network structures: packing-derived (PD) and random geometric graph (RGG) networks at a physiologically relevant connectivity  $z \lesssim 3.5$  [17,23,24]. Importantly, such connectivity lies below the 3D Maxwell isostatic threshold  $z_c = 6$  [25,26], at which central-force networks are marginally stable to linear order, as sketched in Fig. 1. This connectivity-controlled rigidity transition has been extensively studied in spring networks [13,27–30], and is analogous to jamming in granular materials [31–33], although the critical exponents differ.

For PD networks, we use a jammed packing of spheres to create an off-lattice network. We randomly distribute a 50:50 bidisperse mixture of spherical particles with a size ratio of 1.4 in a periodic cube of size  $W$ , with  $N = W^3$  spheres in total. The particles interact via a repulsive harmonic potential [22,34,35]. We start by swelling the particles until the pressure becomes finite, which yields a network with  $z \approx 2d = 6$ . We then randomly remove bonds to obtain the desired connectivity  $z < 6$ . For RGG networks, we randomly distribute nodes in a cube with a side length  $W$  before connecting pairs of nodes according to a distance-dependent probability distribution [36] until the desired connectivity is reached. More details on the RGG model are provided in the Supplemental Material [37].

The network elastic energy  $H$  consists of stretching and bending contributions

$$H = \frac{\mu}{2} \sum_{ij} \frac{(\ell_{ij} - \ell_{ij,0})^2}{\ell_{ij,0}} + \frac{\kappa_b}{2} \sum_{ijk} \frac{(\theta_{ijk} - \theta_{ijk,0})^2}{\ell_{ijk,0}}, \quad (1)$$

where  $\mu$  is the stretching modulus of the individual bonds,  $\ell_{ij,0}$  is the initial bond length prior to any deformation,  $\ell_{ij}$  is the current bond length,  $\kappa_b$  is the bending stiffness of fibers,  $\theta_{ijk,0}$  is the initial angle between two adjacent bonds  $ij$  and

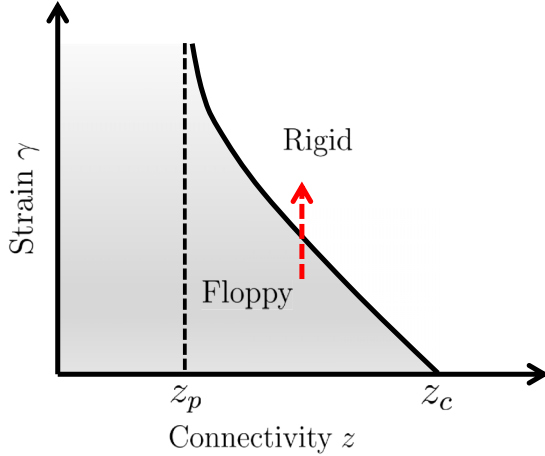


FIG. 1. Schematic phase diagram for central-force networks. Networks with an average connectivity below the percolation threshold  $z_p$  are disconnected, hence there is no mechanical response at any strain value. Networks with  $z > z_c$ , however, are stable at zero strain. In the intermediate regime, with  $z_p < z < z_c$ , networks are floppy at zero strain but can be rigidified by applying strain beyond a finite threshold that depends on the network's connectivity and geometry. The red arrow indicates the nonlinear transition in subisostatic networks that is the subject of this study.

$jk$  prior to any deformation,  $\theta_{ijk}$  is the current angle between adjacent bonds  $ij$  and  $jk$ , and  $\ell_{ijk,0} = \frac{\ell_{ij,0} + \ell_{jk,0}}{2}$  is the initial average bond length of bonds  $ij$  and  $jk$ . We set  $\mu = 1$  and vary the dimensionless bending stiffness  $\kappa = \kappa_b/\mu\ell_c^2$ , where  $\ell_c$  is the average initial bond length. All lengths in the system are in units of  $\ell_c$ . We also note that there are no excluded volume interactions between fibers or the network nodes in our models.

To study the mechanical transition, we apply a simple shear deformation  $\gamma$  in a stepwise manner in the  $x$ - $z$  plane using Lees-Edwards boundary conditions [38]. Although we focus on shear, we note that uniaxial and bulk deformations can also rigidify such networks [39–43]. Using the FIRE algorithm [44], we minimize the elastic energy defined in Eq. (1) at each strain step and calculate the stress tensor as [21]

$$\sigma_{\alpha\beta} = \frac{1}{2V} \sum_{ij} f_{ij,\alpha} r_{ij,\beta}, \quad (2)$$

where  $V$  is the volume of the system,  $f_{ij,\alpha}$  is the  $\alpha$  component of the force exerted on node  $i$  by node  $j$ , and  $r_{ij,\beta}$  is the  $\beta$  component of the displacement vector connecting nodes  $i$  and  $j$ . We then compute the differential shear modulus as  $K = \partial\sigma_{xz}/\partial\gamma$ , which is an energy per volume and is given here in units of  $\mu/\ell_c^{d-1}$ . Unless otherwise stated, quantities reported throughout this Letter correspond to averages over 40 random realizations.

*Scaling relation.* When we apply sufficiently large shear strain to a subisostatic network with central-force interactions (red arrow in Fig. 1), the system undergoes a phase transition from a floppy to a rigid state. At the critical strain  $\gamma_c$ , which is a function of network connectivity  $z$  [13,16], the differential shear modulus  $K$  discontinuously jumps from 0 to a finite value  $K_c$  [15,43,45]. The excess shear modulus

$K - K_c$  exhibits a power-law scaling behavior near  $\gamma_c$ , with  $K - K_c \sim |\Delta\gamma|^f$ , where  $\Delta\gamma = \gamma - \gamma_c$ . Including weak bending interactions between adjacent bonds stabilizes the network in the subcritical regime  $\gamma < \gamma_c$ , such that the floppy-to-rigid transition becomes a transition between bending- and stretching-dominated states. The following Widom-like [46] scaling function captures the mechanics of networks with finite bending stiffness [16],

$$K \approx |\Delta\gamma|^f \mathcal{G}_\pm \left( \frac{\kappa}{|\Delta\gamma|^\phi} \right), \quad (3)$$

in which the positive and negative branches of the scaling function  $\mathcal{G}_\pm$  correspond to  $\Delta\gamma > 0$  and  $\Delta\gamma < 0$ , respectively. For  $\gamma < \gamma_c$  and  $\kappa/|\Delta\gamma|^\phi \ll 1$ , the shear modulus scales as  $K \sim \kappa|\Delta\gamma|^{-\lambda}$  with  $\lambda = \phi - f$ . We note that the continuity of  $K$  as a function of  $\gamma$  requires that  $K \sim \kappa^{f/\phi}$  when  $\kappa/|\Delta\gamma|^\phi$  is large.

To relate the scaling exponents near the critical strain  $\gamma_c$ , we follow the approach of Kadanoff [47] for the elastic energy per node  $h$  as a function of the small parameters  $t = \gamma - \gamma_c$  and  $\kappa$  [21]. Rescaling the system by a factor  $L$  results in a renormalized energy  $h(t', \kappa') = L^d h(t, \kappa)$ , in which  $t'$  and  $\kappa'$  are the renormalized variables after transformation and  $d$  is dimensionality. We assume that  $t' = tL^x$  and  $\kappa' = \kappa L^y$  near the critical point, with positive  $x$  and  $y$ . We can therefore write the elastic energy per node as [21]

$$h(t, \kappa) = L^{-d} h(tL^x, \kappa L^y). \quad (4)$$

We find the differential shear modulus  $K \sim L^{-d+2x} h_{2,0}(tL^x, \kappa L^y)$  from the second derivative with respect to  $\gamma$  or  $t$ , in a way analogous to the heat capacity in a thermal phase transition, in which case differentiation is with respect to the temperature. Here,  $h_{2,0}$  represents the second partial derivative of  $h$  with respect to the first argument. So far, the rescaling factor  $L$  is simply a mathematical parameter that has not been specified. Thus, physical quantities such as  $K$  cannot depend on  $L$ , from which the form of Eq. (3) follows [48]. By choosing  $L = |t|^{-1/x}$ , we find that  $f = d/x - 2$  for  $\gamma > \gamma_c$ . We also identify the correlation length  $\xi \sim L \sim |t|^{-y}$  and the scaling relations [21,48]

$$f = d - 2 \quad \text{and} \quad \phi = yv. \quad (5)$$

The first of these is a hyperscaling relation that is of particular importance for the appearance of the dimensionality  $d$  of the system. This can only be satisfied for mean-field systems at a particular  $d = d_u$ , which sets the upper critical dimension. Only for dimensionalities below this are non-mean-field critical exponents possible.

*Results.* In order to find the critical exponent  $f$ , care must be taken to account for finite-size effects. For a finite system, only when the system size exceeds the correlation length  $\xi$ , i.e.,  $W|t|^v \gtrsim 1$ , will the thermodynamic properties approximate those of the thermodynamic limit. In the opposite limit  $W|t|^v \lesssim 1$ , which occurs close to  $t = 0$ , correlations are limited and analytic behavior is expected. Thus, we determine the critical exponents only for  $W \gtrsim \xi$ . For small  $t > 0$ , we expect the shear modulus to vary with system size  $W$  as [45]

$$K - K_c = W^{-f/v} \mathcal{F}(tW^{1/v}). \quad (6)$$

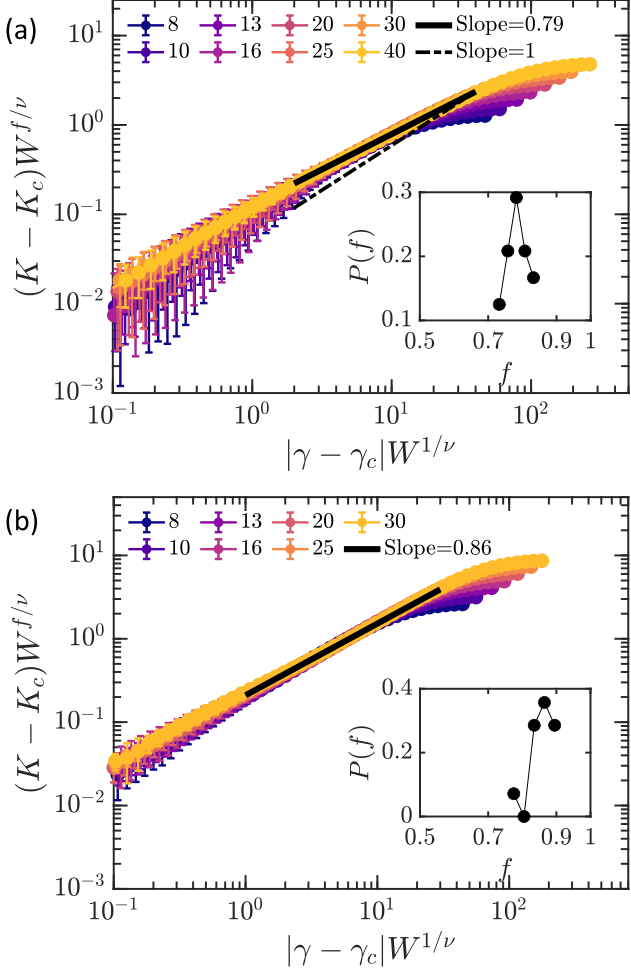


FIG. 2. (a) Finite-size analysis of  $K$  for the PD model at  $z = 3.3$  with  $\kappa = 0$ . In the critical region, we obtain  $f = 0.79 \pm 0.03$ . (b) Similar finite-size scaling analysis for PD networks at a different connectivity  $z = 4.0$ . We find an exponent of  $f = 0.86 \pm 0.04$  in the critical regime. For both models, an apparent exponent of 1.0 is observed in the finite-size-dominated region, consistent with analytic behavior. The insets show the distribution of the exponent  $f$ .

Here,  $\mathcal{F}(x)$  is a scaling function that is expected to increase as  $\sim x^f$  for large arguments, in order to obtain a well-defined thermodynamic limit. Figure 2 shows the finite-size analysis corresponding to this. Here, the sample-dependent critical strain  $\gamma_c$  is found using the bisection method [43,45]. For PD networks at  $z = 3.3$  of size  $W = 40$  at strains beyond the regime dominated by finite-size effects (i.e.,  $W \gtrsim \xi$ ), we find  $f = 0.79 \pm 0.03$ , where the errors are standard deviations for 20 random realizations [37]. Upon increasing the connectivity to  $z = 4.0$ , the resulting data are consistent with a slightly larger  $f = 0.86 \pm 0.04$ , which is obtained by averaging 20 samples of size  $W = 30$  (see Fig. 2). The distributions of the  $f$  exponent are shown as insets in Fig. 2. For the RGG model at  $z = 3.3$  we find  $f = 0.92 \pm 0.02$  using a system size of  $W = 30$  [37].

Similar to 2D models [45], we find that the shear modulus discontinuity  $K_c$  decreases as the system size  $W$  increases [37]. We note that as the network size increases, the regime

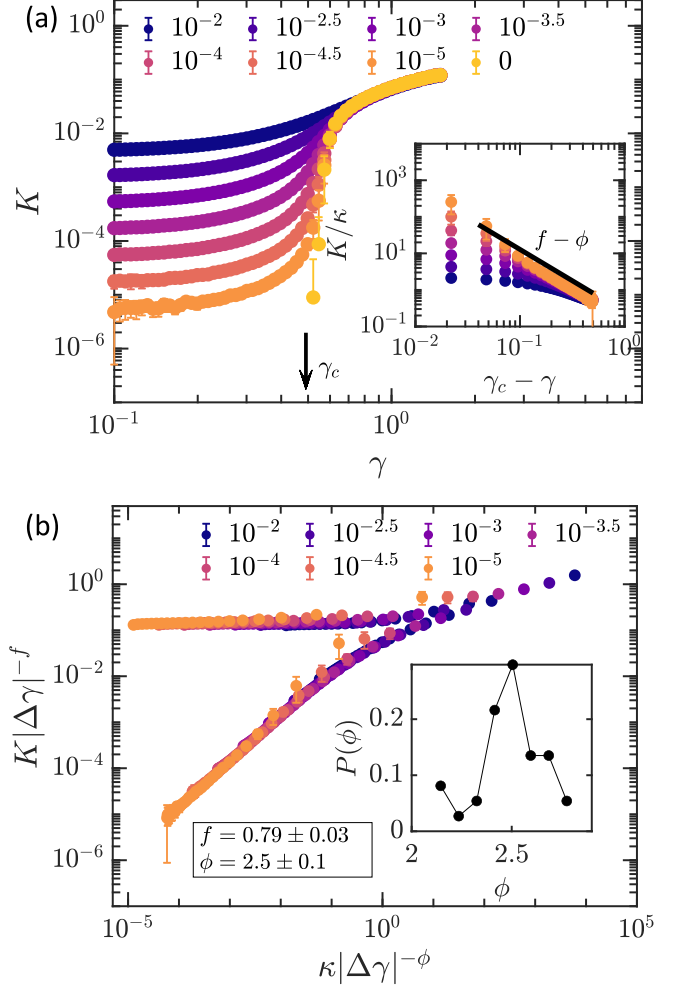


FIG. 3. (a) Differential shear modulus  $K$  for PD networks with  $z = 3.3$  and system size  $W = 30$  at various bending stiffnesses  $\kappa$  as shown in the legend. The inset shows the scaling behavior of  $K$  in the subcritical region, where  $K \sim \kappa |\Delta \gamma|^{-\lambda}$  with  $\lambda = \phi - f$ . (b) Widom-like scaling collapse of  $K$  for data in (a). Using the critical exponents  $f$  and  $\phi$  as explained in the text, we are able to collapse our data based on Eq. (3). The inset shows the distribution of  $\phi$  values.

over which  $f$  can be computed extends to a smaller  $|\Delta \gamma|$ . Here, a non-mean-field exponent of  $f < 1$  is seen. In the finite-size-dominated regime, however, the data are consistent with  $f = 1$ , which can be explained by a leading first term in the scaling function that becomes analytic when  $W \lesssim \xi$ , as previously seen in 2D fiber networks [45] and jammed systems [49].

In Fig. 3(a), we plot the shear modulus versus strain for packing-derived networks with finite  $\kappa$  and  $z = 3.3$ . From the value of  $f$  above, we find the critical exponent  $\phi$  in the subcritical regime  $\gamma < \gamma_c$  from Eq. (3). Since  $K$  must be proportional to  $\kappa$  in this regime, we expect  $K \sim \kappa |\Delta \gamma|^{f-\phi}$  (see inset). The distribution of  $\phi$  values with  $\phi = 2.5 \pm 0.1$  is shown in the inset of Fig. 3(b) [37]. Considering Eq. (3), we expect to find a scaling collapse of data in Fig. 3(a) for various  $\kappa$  values to a single master curve. Figure 3(b) shows this Widom-like scaling analysis. As we can see, using the obtained values of  $f$  and  $\phi$ , the data collapse in two branches,

one for the data above  $\gamma_c$ , one for the data below  $\gamma_c$ . A similar analysis for the RGG model with finite bending rigidity results in  $\phi = 2.8 \pm 0.2$  [37].

One of the most striking features of a critical phase transition is the divergence of fluctuations at the critical point, along with the divergent correlation length  $\xi$  for these fluctuations. Here, we measure the nonaffine displacement fluctuations of network nodes under an infinitesimal shear strain, defined as

$$\delta\Gamma = \frac{\langle \|\mathbf{u} - \mathbf{u}^{\text{af}}\|^2 \rangle}{\ell_c^2 \delta\gamma^2}, \quad (7)$$

where  $\mathbf{u}$  is the relaxed position of a network node after applying a small strain  $\delta\gamma$ ,  $\mathbf{u}^{\text{af}}$  is the affinely displaced position of the node under a strain  $\delta\gamma$  from the previous relaxed position,  $\ell_c$  is the average initial bond length of the network, and the angular brackets represent an average over all nodes. For central-force networks, the fluctuations  $\delta\Gamma$  diverge as the network approaches the critical strain [19]. Since the nonaffine displacements  $\delta u^2$  are found by minimizing the energy  $h(t, \kappa)$ , we expect that  $h \sim \kappa \delta u^2 \sim \kappa \delta\gamma^2 \delta\Gamma$  for small but finite  $\kappa$ . Therefore, the fluctuations diverge as [21, 50]

$$\delta\Gamma \sim |\Delta\gamma|^{-\lambda}, \quad (8)$$

where the same  $\lambda = \phi - f$  is observed for both  $\gamma < \gamma_c$  and  $\gamma > \gamma_c$ .

To verify the scaling relation in Eq. (5), we calculate the nonaffine fluctuations  $\delta\Gamma$  for networks with  $\kappa = 0$ , as shown for various system sizes in the Supplemental Material [37]. From Eq. (8), we expect the following scaling form to capture the behavior of  $\delta\Gamma$  in finite simulations [19],

$$\delta\Gamma = W^{\lambda/v} \mathcal{H}(\Delta\gamma W^{1/v}), \quad (9)$$

where  $\mathcal{H}$  is a scaling function and  $\lambda = \phi - f$ . Figure 4(a) shows the finite-size scaling collapse of  $\delta\Gamma$  data using the previously obtained values of  $f$  and  $\phi$ . The correlation length exponent  $v$  is computed from the scaling relation in Eq. (5). Thus, this collapse demonstrates the validity of the hyperscaling relation  $f = d\nu - 2$  in 3D systems. A similar scaling collapse of fluctuations is shown in Fig. 4(b) for the RGG model at  $z = 3.3$ . In order to further test this, we also simulated 3D PD networks at a different connectivity  $z = 4.0$ . The figures for this are shown in the Supplemental Material [37]. The scaling exponents  $f$  and  $\phi$  are slightly larger than the corresponding exponents for networks with  $z = 3.3$ . With these new scaling exponents, we perform a similar finite-size scaling analysis to Fig. 4 and find further evidence that the hyperscaling relation holds. We note that although we deform the networks in the  $x$  direction in the  $x$ - $z$  plane for all the above figures, other shear directions behave similarly since the modulus behaves isotropically at the sizes studied here [37].

*Conclusion.* In this study, we measure the exponents associated with the strain-driven rigidity transition for subisostatic 3D spring networks under applied simple shear. In agreement with previous work on various network architectures [16, 21, 51], we find non-mean-field exponents in the critical regime by performing a systematic finite-size analysis in our 3D computational models. We also demonstrate evidence to

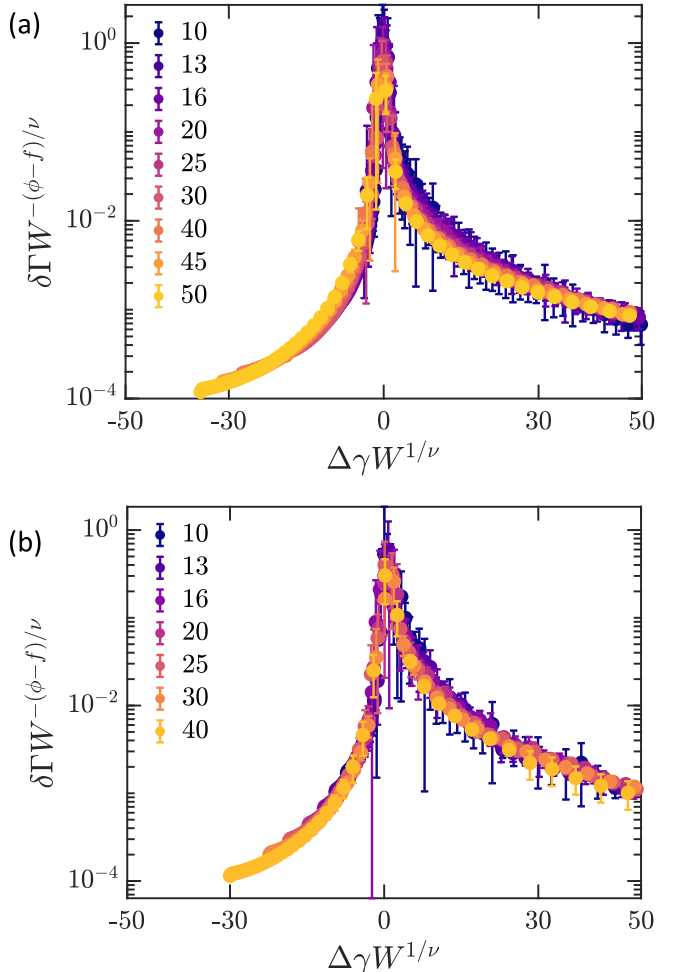


FIG. 4. (a) The finite-size analysis of the nonaffine fluctuations for central-force PD networks at  $z = 3.3$ . As explained in the main text, the scaling exponents  $f$  and  $\phi$  are obtained using shear modulus data in the regimes  $\Delta\gamma > 0$  and  $\Delta\gamma < 0$ , respectively. The correlation length exponent  $v$  is found using the scaling relation  $f = d\nu - 2$ , which results in  $v = 0.93$ . (b) Similar scaling collapse of nonaffine fluctuations as in (a) for a central-force RGG model at  $z = 3.3$  using  $v = (f + 2)/d = 0.97$ .

support a recently proposed hyperscaling relation between critical exponents [21]. Taken together, these results point to an upper critical dimension  $d_u > 3$  for the strain-controlled phase transition that is above three, in stark contrast to the jamming transition [22]. While our focus here has been on the subisostatic transition that is most relevant to fiber networks such as collagen, it is interesting to note that the isostatic critical point corresponding to  $z = 6$  in 3D has also been shown to exhibit non-mean-field exponents [29]. In future work, it will be interesting to study hyperscaling for that transition as well.

*Acknowledgments.* This work was supported in part by the National Science Foundation Division of Materials Research (Grant No. DMR-1826623) and the National Science Foundation Center for Theoretical Biological Physics (Grant No. PHY-2019745).

- [1] L. A. Hough, M. F. Islam, P. A. Janmey, and A. G. Yodh, *Phys. Rev. Lett.* **93**, 168102 (2004).
- [2] M. B. Bryning, D. E. Milkie, M. F. Islam, L. A. Hough, J. M. Kikkawa, and A. G. Yodh, *Adv. Mater.* **19**, 661 (2007).
- [3] B. Dan, G. C. Irvin, and M. Pasquali, *ACS Nano* **3**, 835 (2009).
- [4] D. A. Fletcher and R. D. Mullins, *Nature (London)* **463**, 485 (2010).
- [5] J. A. Pedersen and M. A. Swartz, *Ann. Biomed. Eng.* **33**, 1469 (2005).
- [6] P. A. Janmey, M. E. McCormick, S. Rammensee, J. L. Leight, P. C. Georges, and F. C. MacKintosh, *Nat. Mater.* **6**, 48 (2007).
- [7] M. L. Gardel, J. H. Shin, F. C. MacKintosh, L. Mahadevan, P. Matsudaira, and D. A. Weitz, *Science* **304**, 1301 (2004).
- [8] C. Storm, J. J. Pastore, F. C. MacKintosh, T. C. Lubensky, and P. A. Janmey, *Nature (London)* **435**, 191 (2005).
- [9] D. A. Head, A. J. Levine, and F. C. MacKintosh, *Phys. Rev. Lett.* **91**, 108102 (2003).
- [10] D. A. Head, A. J. Levine, and F. C. MacKintosh, *Phys. Rev. E* **68**, 061907 (2003).
- [11] J. Wilhelm and E. Frey, *Phys. Rev. Lett.* **91**, 108103 (2003).
- [12] M. Das, F. C. MacKintosh, and A. J. Levine, *Phys. Rev. Lett.* **99**, 038101 (2007).
- [13] M. Wyart, H. Liang, A. Kabla, and L. Mahadevan, *Phys. Rev. Lett.* **101**, 215501 (2008).
- [14] C. P. Broedersz and F. C. MacKintosh, *Rev. Mod. Phys.* **86**, 995 (2014).
- [15] M. F. J. Vermeulen, A. Bose, C. Storm, and W. G. Ellenbroek, *Phys. Rev. E* **96**, 053003 (2017).
- [16] A. Sharma, A. J. Licup, K. A. Jansen, R. Rens, M. Sheinman, G. H. Koenderink, and F. C. MacKintosh, *Nat. Phys.* **12**, 584 (2016).
- [17] K. A. Jansen, A. J. Licup, A. Sharma, R. Rens, F. C. MacKintosh, and G. H. Koenderink, *Biophys. J.* **114**, 2665 (2018).
- [18] A. J. Licup, S. Münster, A. Sharma, M. Sheinman, L. M. Jawerth, B. Fabry, D. A. Weitz, and F. C. MacKintosh, *Proc. Natl. Acad. Sci. USA* **112**, 9573 (2015).
- [19] A. Sharma, A. J. Licup, R. Rens, M. Vahabi, K. A. Jansen, G. H. Koenderink, and F. C. MacKintosh, *Phys. Rev. E* **94**, 042407 (2016).
- [20] J. L. Shivers, J. Feng, A. Sharma, and F. C. MacKintosh, *Soft Matter* **15**, 1666 (2019).
- [21] J. L. Shivers, S. Arzash, A. Sharma, and F. C. MacKintosh, *Phys. Rev. Lett.* **122**, 188003 (2019).
- [22] C. P. Goodrich, S. Dagois-Bohy, B. P. Tighe, M. van Hecke, A. J. Liu, and S. R. Nagel, *Phys. Rev. E* **90**, 022138 (2014).
- [23] S. B. Lindström, D. A. Vader, A. Kulachenko, and D. A. Weitz, *Phys. Rev. E* **82**, 051905 (2010).
- [24] S. B. Lindström, A. Kulachenko, L. M. Jawerth, and D. A. Vader, *Soft Matter* **9**, 7302 (2013).
- [25] J. C. Maxwell, *Trans. R. Soc. Edinburgh* **26**, 1 (1870).
- [26] C. R. Calladine, *Int. J. Solids Struct.* **14**, 161 (1978).
- [27] S. Feng and M. Sahimi, *Phys. Rev. B* **31**, 1671 (1985).
- [28] S. Arbabi and M. Sahimi, *Phys. Rev. B* **38**, 7173 (1988).
- [29] C. P. Broedersz, X. Mao, T. C. Lubensky, and F. C. MacKintosh, *Nat. Phys.* **7**, 983 (2011).
- [30] J. Feng, H. Levine, X. Mao, and L. M. Sander, *Soft Matter* **12**, 1419 (2016).
- [31] M. E. Cates, J. P. Wittmer, J.-P. Bouchaud, and P. Claudin, *Phys. Rev. Lett.* **81**, 1841 (1998).
- [32] A. J. Liu and S. R. Nagel, *Nature (London)* **396**, 21 (1998).
- [33] M. van Hecke, *J. Phys.: Condens. Matter* **22**, 033101 (2010).
- [34] C. S. O'Hern, S. A. Langer, A. J. Liu, and S. R. Nagel, *Phys. Rev. Lett.* **88**, 075507 (2002).
- [35] C. S. O'Hern, L. E. Silbert, A. J. Liu, and S. R. Nagel, *Phys. Rev. E* **68**, 011306 (2003).
- [36] F. Beroz, L. M. Jawerth, S. Münster, D. A. Weitz, C. P. Broedersz, and N. S. Wingreen, *Nat. Commun.* **8**, 16096 (2017).
- [37] See Supplemental Material at <http://link.aps.org/supplemental/10.1103/PhysRevE.104.L022402> for distributions of the critical strain, the fitting procedure, the two-branch behavior in the RGG model, finite-size analysis of the shear modulus discontinuity, unscaled data of differential nonaffinity parameter, and the effect of different shear directions.
- [38] A. W. Lees and S. F. Edwards, *J. Phys. C* **5**, 1921 (1972).
- [39] M. Sheinman, C. P. Broedersz, and F. C. MacKintosh, *Phys. Rev. E* **85**, 021801 (2012).
- [40] A. S. G. van Oosten, M. Vahabi, A. J. Licup, A. Sharma, P. A. Galie, F. C. MacKintosh, and P. A. Janmey, *Sci. Rep.* **6**, 19270 (2016).
- [41] M. Vahabi, A. Sharma, A. J. Licup, A. S. G. van Oosten, P. A. Galie, P. A. Janmey, and F. C. MacKintosh, *Soft Matter* **12**, 5050 (2016).
- [42] S. Arzash, J. L. Shivers, A. J. Licup, A. Sharma, and F. C. MacKintosh, *Phys. Rev. E* **99**, 042412 (2019).
- [43] M. Merkel, K. Baumgarten, B. P. Tighe, and M. L. Manning, *Proc. Natl. Acad. Sci. USA* **116**, 6560 (2019).
- [44] E. Bitzek, P. Koskinen, F. Gähler, M. Moseler, and P. Gumbsch, *Phys. Rev. Lett.* **97**, 170201 (2006).
- [45] S. Arzash, J. L. Shivers, and F. C. MacKintosh, *Soft Matter* **16**, 6784 (2020).
- [46] B. Widom, *J. Chem. Phys.* **43**, 3898 (1965).
- [47] L. P. Kadanoff, *Phys. Phys. Fiz.* **2**, 263 (1966).
- [48] L. P. Kadanoff, W. Götze, D. Hamblen, R. Hecht, E. A. S. Lewis, V. V. Palcianuskas, M. Rayl, J. Swift, D. Aspnes, and J. Kane, *Rev. Mod. Phys.* **39**, 395 (1967).
- [49] C. P. Goodrich, A. J. Liu, and S. R. Nagel, *Phys. Rev. Lett.* **109**, 095704 (2012).
- [50] C. P. Broedersz, Ph.D. thesis, Vrije Universiteit, Amsterdam, 2011.
- [51] R. Rens, M. Vahabi, A. J. Licup, F. C. MacKintosh, and A. Sharma, *J. Phys. Chem. B* **120**, 5831 (2016).